# The Influence of Amine Structure on the Mechanism of CO<sub>2</sub> Facilitated Transport Across Amine-Functionalized Polymer Membranes: An *Operando* Spectroscopy Study Hui Xu,<sup>a‡</sup> Sarah G. Pate,<sup>b‡</sup> and Casey P. O'Brien<sup>b\*</sup> <sup>a</sup>Department of Chemistry and Biochemistry, University of Notre Dame, Notre Dame, IN 46556, USA <sup>b</sup>Department of Chemical and Biomolecular Engineering, University of Notre Dame, Notre Dame, IN 46556, USA <sup>‡</sup> These two authors contributed equally to this work. \*Corresponding Author Email Address: cobrie23@nd.edu

The influence of the amine structure (secondary, tertiary, pyridinic) in amine-functionalized polymeric membranes on the mechanism of CO<sub>2</sub> transport across the membrane is investigated in this work using *operando* surface enhanced Raman spectroscopy (SERS) and *in-situ* transmission FTIR spectroscopy. Specifically, the mechanism of CO<sub>2</sub> transport across poly-N-methyl-N-vinylamine (PMVAm), poly-N, N-dimethyl-N-vinylamine (PDVAm), and poly(4-vinylpyridine) (P4VP) membranes was investigated by measuring CO<sub>2</sub> permeances/selectivities of the membranes and simultaneously detecting CO<sub>2</sub> transport intermediates (e.g., carbamate, bicarbonate) formed in the membrane under operating conditions using SERS and FTIR spectroscopy. While permeation measurements suggest that CO<sub>2</sub> moves across all membranes via a facilitated transport mechanism, *operando* SERS and *in-situ* FTIR results suggest that the

Abstract

molecular-level details of the facilitated transport process are highly sensitive to the structure of the amine functional group. For membranes with secondary (PMVAm) and tertiary (PDVAm) amines, CO<sub>2</sub> moves across the membrane as a mixture of both carbamate and bicarbonate species. For P4VP, which has pyridinic amine groups, no CO<sub>2</sub>-derived intermediates were detected suggesting a new facilitated transport mechanism involving weak interactions between CO<sub>2</sub> and the pyridinic nitrogen group without transformation of CO<sub>2</sub> into carbamate, bicarbonate, or other intermediate species. Such a facilitated transport mechanism has not been reported in the literature to our knowledge.

30 Keywords: Operando spectroscopy, facilitated transport, carbon capture, polymer membrane.

#### 1. Introduction

Amine-functionalized polymer membranes are attractive for CO<sub>2</sub> capture/separation applications because of their unique facilitated transport mechanism. In this transport mechanism, reactive amines selectively facilitate CO<sub>2</sub> transport across the membrane without influencing the transport of other gases to give rapid and selective CO<sub>2</sub> separation from mixed gas streams. Studies show that the CO<sub>2</sub> separation performance of amine-based facilitated transport membranes is sensitive to the structure of the amine functional group (e.g., primary, secondary, tertiary) [1-3]. For example, Ho et al. [1] showed that the degree of steric hindrance at the amine functional group, which can be controlled by chemically attaching alkyl groups to the pendant amine group, has a significant impact on the CO<sub>2</sub> separation performance of the membrane, with a moderate degree of steric hindrance yielding optimal performance. However, the influence of the amine structure/type on the fundamental mechanism of CO<sub>2</sub> facilitated transport is not well understood on the molecular level, which hinders rational design of high-performance membranes.

Ho et al. [1] postulated that the structure (e.g., degree of steric hindrance) of the amine functional group influences the performance of the membrane by affecting the CO<sub>2</sub> transport mechanism and consequently the CO<sub>2</sub> loading (i.e., solubility) of the membrane. Based on a mechanism originally proposed by Caplow [4] and Danckwerts [5], Ho et al. [1] proposed that the first step in the CO<sub>2</sub> transport mechanism is the reaction of CO<sub>2</sub> with the amine to form a zwitterion intermediate, equation (1):

$$CO_2 + R - NH_2 \rightleftharpoons R - NH_2^+ COO^- \tag{1}$$

For an unhindered amine, the zwitterion can be deprotonated by another amine to form a carbamate ion  $(R - NHCOO^{-})$  according to equation (2):

53 
$$R - NH_2^+COO^- + R - NH_2 \rightarrow R - NHCOO^- + R - NH_3^+$$
 (2)

Combining equations (1) and (2) to give the overall reaction stoichiometry, equation (3):

$$CO_2 + 2R - NH_2 \rightleftharpoons R - NH_3^+ + R - NHCOO^-$$
 (3),

the maximum CO<sub>2</sub> loading for an unhindered amine is only 0.5 mol CO<sub>2</sub> per mol of amine. For a sterically-hindered amine, the alkyl group attached to the amine destabilizes the carbamate ion, and a different mechanism has been proposed in which the sterically-hindered amine group catalyzes the transformation of CO<sub>2</sub> with H<sub>2</sub>O to give a bicarbonate ion, according to equation (4):

60 
$$CO_2 + R_1 - NH - R_2 + H_2O \rightleftharpoons R_1 - NH_2^+ - R_2 + HCO_3^-$$
 (4)

Thus, the stoichiometric CO<sub>2</sub> loading of a sterically-hindered amine (1.0) is double that of an unhindered amine (0.5). In other words, Ho et al. [1] posited that the performance of amine-functionalized membranes with sterically-hindered amine groups was greater than that of unhindered amines because the CO<sub>2</sub> loading (i.e., solubility) of sterically-hindered amines that convert CO<sub>2</sub> to bicarbonate is higher than that of unhindered amines that transport CO<sub>2</sub> primarily as carbamate species. This explanation is consistent with studies on CO<sub>2</sub> reactions with aqueous amine solutions [6-8].

While the CO<sub>2</sub> facilitated transport mechanism proposed by Ho et al. [1, 7, 8] can help to understand differences across a homologous series of membranes with similar amine structures, there is a wide and diverse range of amine groups that could be incorporated into polymeric membranes, and the molecular scale interactions of CO<sub>2</sub> with different amine functional groups is not well understood. There are amine sorbent studies utilizing solid or liquid amine materials with different structures which have shown spectral differences when interacting with CO<sub>2</sub>, thus indicating different CO<sub>2</sub> intermediate species [9-23]. These adsorption studies showed that CO<sub>2</sub> adsorbs as carbamate, carbamic acid, bicarbonate, or a combination of these depending on the

amine structure [9, 10, 17, 18]. There is a need to apply similar spectroscopic approaches to membrane separation systems (e.g., [24-29]) to better understand the fundamental CO<sub>2</sub> transport mechanism and ultimately to enable a more rational design of high-performance membranes than current trial-and-error approaches.

To probe the molecular-scale mechanisms of CO<sub>2</sub> transport across amine-functionalized membranes, we have recently developed new *operando* transmission FTIR spectroscopy [30] and *operando* surface enhanced Raman spectroscopy (SERS) [31, 32] tools that enable detection of CO<sub>2</sub> transport intermediates (e.g., carbamate, bicarbonate) formed in the bulk of the membrane while simultaneously measuring CO<sub>2</sub> permeation rates under realistic permeation conditions. We demonstrated the utility of these new *operando* spectroscopy tools by showing that CO<sub>2</sub> moves across polyvinylamine (PVAm; see **Figure 1**), an archetypal facilitated transport membrane with primary amine groups, mainly as carbamate species. This observation was consistent with the mechanism proposed by Ho et al. [33] in which a primary amine such as that in PVAm should interact with CO<sub>2</sub> to form a carbamate ion.

Figure 1. Polymer structures of PVAm, PMVAm, PDVAm, and P4VP.

In this work, we investigate the influence of the structure of the amine group in polymeric facilitated transport membranes on the CO<sub>2</sub> transport mechanism using *operando* SERS and *insitu* FTIR spectroscopy. Specifically, we investigate the mechanism of CO<sub>2</sub> transport across poly-

N-methyl-N-vinylamine (PMVAm), poly-N, N-dimethyl-N-vinylamine (PDVAm), and poly(4-vinylpyridine) (P4VP) (Figure 1). For both PMVAm and PDVAm, which have secondary and tertiary amine groups, respectively, we observe intermediate species that are consistent with carbamate species and bicarbonate species. For P4VP, which has pyridinic amine groups, no CO2-derived intermediate species were detected even though permeation measurements were consistent with a facilitated transport mechanism. It is possible that P4VP facilitates CO2 transport by a new mechanism in which the pyridinic nitrogen group facilitates CO2 transport via weak CO2-nitrogen interactions rather than by converting CO2 to carbamate, bicarbonate, or other intermediate species. This work provides direct spectroscopic evidence that the mechanism of CO2 transport across amine-functionalized membranes is indeed highly sensitive to the structure of the amine functional group. Understanding the relationships between polymer structures, operating conditions, and separation performance on a molecular level will promote the rational design of membranes which have high CO2 permeation rates, high selectivity to CO2, and are stable for extended periods of time.

#### 2. Experimental

#### 2.1 Materials

N-vinylformamide (NVF, ≥96% stabilized), hydrochloric acid (HCl, 37%), ethanol (denatured, anhydrous), methanol (≥99.8%), acetone (≥99.5%), and potassium hydroxide (KOH) were purchased from VWR. Azobisisobutyronitrile (AIBN, 97%) and iodomethane (99%) were purchased from Sigma-Aldrich. Strong base anion-exchange resin (Purolite® A600OH) was purchased from APS WATER. All the chemicals, except NVF were used as received without further purification. Poly(4-vinylpyridine) (P4VP, ~160,000 MW) and polystyrene (PS, ~280,000 MW) were purchased from Sigma-Aldrich and used as received without further purification. CO<sub>2</sub>,

N<sub>2</sub>, CH<sub>4</sub>, and Ar gas cylinders (purity of ≥99.99%) were purchased from Airgas. Polyvinylidene fluoride (PVDF) and polypropylene (PP) porous substrates were used. PVDF was provided by the Phillip Lab at the University of Notre Dame, but originally supplied by Nanostone. Celgard donated the PP sample (Celgard 2075) with a thickness of 20 μm. PVDF was used as received. Celgard 2075 polypropylene (PP) was cleaned by soaking in ethanol for four hours followed by soaking in deionized water for four hours to knock out the ethanol in the pores and dried in a fume hood overnight.

## 2.2 PVAm, PMVAm, PDVAm Polymer Synthesis and Characterization

Polyvinylamine (PVAm) was synthesized utilizing a previously reported procedure [30-32]. The N-vinylformamide (NVF) monomer was purified by vacuum distillation at 40 °C to remove the inhibitor. Purified NVF (20 g) was dissolved in 30 mL of deionized (DI) water in a 20 mL round-bottom flask. The solution was heated to 50 °C and degassed with nitrogen for 1 h before the addition of AIBN (initiator). The polymerization process was carried out under nitrogen at 50 °C for 3 h. Acidic hydrolysis was performed with 2 equivalents of 2 M HCl aqueous solution at 70 °C for 5 h under nitrogen following the polymerization. The polymer was then precipitated with ethanol and dried in a vacuum oven at room temperature for 2 days. Subsequently, the dried polymer was dissolved in DI water at 60 °C for 24 h to prepare a 3 wt% solution. The pH of the solution was adjusted to 11 using strong base anion-exchange resin, followed by vacuum filtration to remove the resin.

Poly(N-methyl-N-vinylamine) (PMVAm) was synthesized from PVAm through a substitution reaction between the amine groups of PVAm and iodomethane with KOH as the catalyst and acid acceptor [3]. Following the pH adjustment of PVAm, the water was removed by

rotary evaporation. Then, a 2 wt% solution was prepared by dissolving the dried PVAm in a methanol/water solvent mixture at a 4:1 weight ratio. KOH and iodomethane were added in equivalent amounts to the solution at room temperature and refluxed at 55°C for 48 h in a light blocking environment. The polymer was purified by dialysis in deionized DI water for 2 days, and then precipitated in an ethanol/acetone solution with a 1:1 weight ratio and a pH of 2 for further purification. The dried polymer was dissolved in DI water to form a 3 wt% solution, and then the pH was adjusted to 11. The PMVAm structure was characterized using attenuated total internal reflectance-Fourier transform infrared (ATR-FTIR) (FT/IR-6300, Jasco) with a spectral resolution of 4 cm<sup>-1</sup> and 64 scans-per-spectrum, and <sup>1</sup>H NMR spectroscopy (Bruker AVANCE III HD 400 Nanobay spectrometer). Figure S1 shows a comparison of the FTIR spectra of PVAm and PMVAm. The FTIR spectrum of PMVAm shows two bands at 1172 cm<sup>-1</sup> and 2779 cm<sup>-1</sup>, which are not present in the FTIR spectrum of PVAm, that can be attributed to the C-N stretching vibration and the C-H stretching vibration, respectively, of the methyl group of PMVAm [3]. The <sup>1</sup>H NMR spectrum of PMVAm (**Figure S2**) shows a broad peak corresponding to a methyl group at 3.03 ppm, with an integration ratio of ~3:2 compared with the methylene group on the backbone at 2.12 ppm. Both the FTIR and <sup>1</sup>H NMR results are consistent with the PMVAm structure shown in **Figure 1**.

140

141

142

143

144

145

146

147

148

149

150

151

152

153

154

155

156

157

158

159

160

161

162

Poly(N,N-dimethyl-N-vinylamine) (PDVAm) was synthesized using a similar method to the PMVAm synthesis. To synthesize PDVAm, a 2 wt% solution was prepared by dissolving the dried PVAm in a methanol/water solvent mixture at a 3:1 weight ratio. Two equivalent amounts of KOH and iodomethane were added at room temperature and refluxed in a shaded environment at 55°C for 5 days. After the reaction, the polymer was purified via dialysis in DI water for 2 days, and then precipitated in an ethanol/acetone solution at a 1:1 weight ratio with a pH of 2. A 3 wt%

solution was formed by dissolving the dried polymer in DI water. The pH was adjusted to 11 to use for membrane preparation. The PDVAm structure was also characterized FTIR and <sup>1</sup>H NMR spectroscopy. Similar to PMVAm, bands at 1172 cm<sup>-1</sup> and 2779 cm<sup>-1</sup>, related to the methyl group, are detected in the FTIR spectrum of PDVAm (**Figure S1**). A broad peak corresponding to methyl groups was observed at 3.00 ppm in the <sup>1</sup>H NMR (**Figure S3**), which has an integration ratio of ~6:2 with the methylene group on the backbone at 2.12 ppm. Thus, both the FTIR and <sup>1</sup>H NMR results are consistent with the PDVAm structure shown in **Figure 1**. While the FTIR and <sup>1</sup>H NMR spectra of PMVAm and PDVAm are consistent with the corresponding structures shown in **Figure 1**, the ratio of the <sup>1</sup>H NMR peaks associated with methylene group and the backbone peak are not exactly 6:2 (6.0:2.4) and 3:2 (3.0:2.2), respectively, and thus it is possible that a small fraction of the primary amine sites of PVAm were not fully converted to PMVAm and PDVAm.

## 2.3 Membrane Preparation

For membrane preparation, PMVAm and PDVAm solutions were concentrated to 3 wt% solutions, while P4VP was concentrated to a 20 wt% solution (10 wt% P4VP solution was used for *in-situ* transmission FTIR measurements); these concentrations provide sufficient solution viscosities to result in better adhesion for casting thin films [34]. The concentrated solutions were knife cast onto PVDF with a wet thickness of 178 µm, or 51 µm on cleaned PP supports where the PP-supported materials were transmission FTIR compatible [30]. The casting solution for SERS-active membranes was prepared by incorporating silver nanoparticles into each polymer solution (20.4 mg/mL for PMVAm and PDVAm, and 10.2 mg/mL for P4VP) to enhance the Raman scattering in the thin active layer [31]. All composite membranes were dried overnight in a fume hood under ambient conditions. The SERS-active membranes were installed to the SERS permeation cell with an active area of 2.2 cm<sup>2</sup>. The PP-supported membranes were mounted to an

aluminum disc using JB Weld Epoxy to install into the FTIR permeation cell with an active area of 0.79 cm<sup>2</sup> for PMVAm and PDVAm, while P4VP was mounted with an active area of 1.13 cm<sup>2</sup>.

Based on our prior work [32] preparing PVAm membranes using an identical procedure used in this work to prepare PMVAm and PDVAm membranes (3 wt% solutions, 178 μm wet thickness on PVDF), we estimate the thickness of the PMVAm and PDVAm membranes used for *operando* SERS measurements to be ~2 μm thick. The thickness of the PMVAm and PDVAm membranes supported on PP for *in-situ* transmission FTIR measurements is unknown; however, the thickness is expected to be significantly less than ~2 μm thick due to the lower wet thickness (51 μm) used during knife casting. For transmission FTIR measurements, thinner membranes are required to avoid saturation of the vibrational bands in the fingerprint region [30]. The thickness of the P4VP membranes is also unknown, but is expected to be significantly greater than ~2 μm thick given the higher concentration of the P4VP casting solution (20%).

# 2.4 Operando SERS Measurements

Operando SERS measurements were conducted using a Raman spectroscopic permeation cell, as described in our previous work [31], which is employed to measure gas permeation rates and simultaneously monitor the membrane structure changes under operating conditions (**Figure S4**). The experiments were carried out under room temperature and atmospheric pressure with the feed compositions consisting of 2-99 kPa CO<sub>2</sub>, 2.2 kPa H<sub>2</sub>O, and balance CH<sub>4</sub>. The total feed flow rate was maintained at 10 mL/min, while the Ar sweep flow rate was 148 mL/min. The permeate gas was analyzed using an SRI 8610C Gas Chromatograph equipped with a HayeSep D packed column and a flame ionization detector (FID). During the Raman spectra collection, an incident laser power of 9.8 mW and a 50x Nikon objective were employed.

#### 2.5 In-Situ Transmission FTIR Measurements

Transmission FTIR measurements were performed using an *in-situ* transmission FTIR spectroscopic permeation cell described in our previous work (**Figure S5**) [30]. Spectroscopic measurements were performed at 22 °C and atmospheric pressure. The feed compositions were varied with gas partial pressures of 2-98 kPa CO<sub>2</sub>, 3.7 kPa H<sub>2</sub>O, and balance N<sub>2</sub>. The total feed flow rate was 37.5 mL/min and the Ar sweep flow rate was 10 mL/min. Transmission FTIR spectra were collected with a spectral resolution of 4 cm<sup>-1</sup>, 1.5-minute scan time, and 6 mm aperture size.

#### 3. Results and Discussion

# 3.1 The Mechanism of CO<sub>2</sub> Transport Across PMVAm (Secondary Amine)

The mechanism of CO<sub>2</sub> transport across PMVAm, which has secondary amine functional groups, was investigated using *operando* SERS to detect CO<sub>2</sub> transport intermediates (e.g., carbamate, bicarbonate) formed in the bulk of the PMVAm membrane and simultaneously measure CO<sub>2</sub> permeation rates under realistic operating conditions. For *operando* SERS measurements, Ag nanoparticles were incorporated into 3 wt% aqueous solutions of PMVAm to enhance the Raman scattering intensity (see Section 2.3 for details). The PMVAm solution with Ag nanoparticles was then knife cast onto PVDF supports with a gap of 178 μm. Subsequently, the membrane was employed in our *operando* Raman spectroscopic permeation cell to investigate the structure changes of the membrane during gas separation with varying CO<sub>2</sub> partial pressures. **Figure 2(a)** shows the CO<sub>2</sub> permeance (black; left axis) and CO<sub>2</sub>/CH<sub>4</sub> selectivity (red; right axis) of PMVAm versus CO<sub>2</sub> partial pressure in the feed. The permeation results show that the maximum CO<sub>2</sub> permeance (264 GPU) and CO<sub>2</sub>/CH<sub>4</sub> selectivity (136) were observed at the lowest CO<sub>2</sub> partial pressure of 2 kPa, and both the CO<sub>2</sub> permeance and CO<sub>2</sub>/CH<sub>4</sub> selectivity decrease with increasing

CO<sub>2</sub> partial pressure. This decrease in the CO<sub>2</sub> permeance and CO<sub>2</sub>/CH<sub>4</sub> selectivity with increasing CO<sub>2</sub> partial pressure is consistent with behavior expected for facilitated CO<sub>2</sub> transport [35-37].

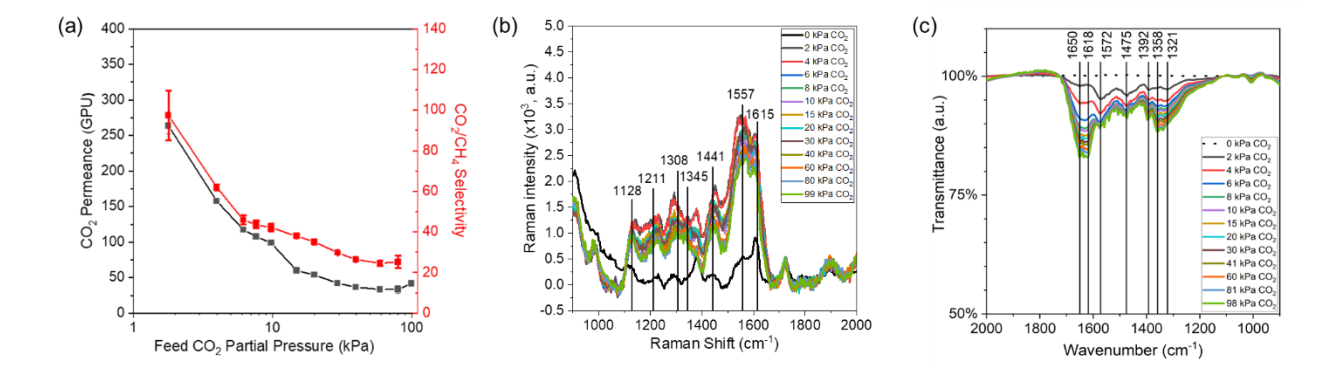


**Figure 2**. CO<sub>2</sub> separation performance and *operando* spectroscopic measurements as a function of feed CO<sub>2</sub> partial pressure for PMVAm where (a) shows the CO<sub>2</sub> permeance (black; left axis) and CO<sub>2</sub>/CH<sub>4</sub> selectivity (red; right axis) and (b) shows the *operando* SERS spectra collected during exposure to a humidified CO<sub>2</sub>/CH<sub>4</sub> feed with 2-99 kPa CO<sub>2</sub>, 2.2 kPa H<sub>2</sub>O, and balance CH<sub>4</sub> at atmospheric pressure and room temperature. (c) *In-situ* transmission FTIR spectra collected during exposure to humidified CO<sub>2</sub>/N<sub>2</sub> with 2-98 kPa CO<sub>2</sub>, 3.7 kPa H<sub>2</sub>O, and balance N<sub>2</sub>.

Figure 2(b) shows the SERS spectra that were collected while the CO<sub>2</sub> permeances/selectivities shown in Figure 2(a) were measured simultaneously. The SERS spectra show several overlapping bands in the 1100 cm<sup>-1</sup> to 1700 cm<sup>-1</sup> range when CO<sub>2</sub> was introduced into the feed side of the PMVAm membrane; these bands were not observed prior to introducing CO<sub>2</sub> (0 kPa CO<sub>2</sub> spectrum). To deconvolute these overlapping bands, the spectrum with a feed CO<sub>2</sub> partial pressure of 99 kPa was normalized by subtracting the spectrum collected prior to introducing CO<sub>2</sub>, and the normalized spectrum was fit to several Gaussian-shaped peaks. The normalized spectrum (Figure S6) shows at least seven bands located between 1100 cm<sup>-1</sup> to 1700 cm<sup>-1</sup>. Assignment of these peaks is based on a comparison of the peak positions with the literature. The peak positions and assignments, with references to the literature, are summarized in Table 1.

Table 1. Raman and IR bands formed during exposure to humidified CO<sub>2</sub> and their assignments
 for PMVAm.

Raman Shift (cm <sup>-1</sup> )	Wavenumber (cm <sup>-1</sup> )	Band Assignment	Attributed Species	Refs.
	1650	COO <sup>-</sup> asymmetric stretch from bicarbonate or C=O stretching from carbamic acid (dimer)	Bicarbonate Ion or Carbamic Acid	[19]
	1617	NH <sub>2</sub> <sup>+</sup> asymmetric bending	Ammonium Ion	[11, 12, 19-22]
1615		Asymmetric C-O stretch in bicarbonate	Bicarbonate Ion	[18, 40, 41, 43- 45]
1557	1579	-COO <sup>-</sup> asymmetric stretching from carbamate	Carbamate Ion	[14, 39, 43] [10, 12, 13, 19, 47]
	1479	NH <sub>2</sub> <sup>+</sup> symmetric bending and NH <sup>+</sup> bending	Ammonium Ion	[9, 12, 13, 17, 19, 21]
	1446	-COO symmetric stretching (secondary band)	Carbamate Ion	[12, 13, 19, 21]
1441		NH <sub>2</sub> <sup>+</sup> bending mode/-COO symmetric stretching	Ammonium Ion or bicarbonate Ion	[38, 39]
	1395	-COO <sup>-</sup> symmetric stretching from carbamate	Carbamate Ion	[12, 15, 16, 19, 21]
1345	1345	C-O symmetric stretch from bicarbonate	Bicarbonate Ion	[18, 38- 45] [14, 19, 21]
1308		NCOO <sup>-</sup> stretching vibration from carbamate (secondary band) or C-OH bend from bicarbonate	Carbamate Ion or Bicarbonate Ion	[14, 38- 41]
1211		Unknown	Unknown	
1128		C-N-C asymmetric stretching of carbamate ion or neutral secondary amine	Carbamate Ion or neutral secondary amine	[40, 46]

The band at 1308 cm<sup>-1</sup> is consistent with the N-COO- stretching vibration of carbamate [38, 39] or C-OH bending of HCO<sub>3</sub><sup>-</sup> [14, 40, 41]. The bands at 1345 cm<sup>-1</sup> and 1615 cm<sup>-1</sup> can be attributed to the C-O symmetric vibration of HCO<sub>3</sub><sup>-</sup> [18, 38-45], and the asymmetric vibration of C-O bonds in HCO<sub>3</sub><sup>-</sup> [18, 40, 41, 43-45], respectively. The band at 1441 cm<sup>-1</sup> may be attributed to NH<sub>2</sub><sup>+</sup> bending [38] or -COO<sup>-</sup> symmetric stretching of bicarbonate [39]. The band at 1557 cm<sup>-1</sup> is consistent the asymmetric stretching of COO<sup>-</sup> in carbamate [14, 39, 43]. The band at 1128 cm<sup>-1</sup> may be contributed by the C-N-C asymmetric stretching of carbamate ion or neutral secondary amine [40, 46], but there is limited literature to support this assignment. The band at 1211 cm<sup>-1</sup> is more difficult to assign because there are almost no Raman spectra reported in literature for the reaction of secondary amines with CO<sub>2</sub>. These *operando* SERS results suggest that the CO<sub>2</sub> moves across PMVAm as both carbamate and bicarbonate intermediates.

In addition to *operando* SERS measurements, the mechanism of CO<sub>2</sub> transport across PMVAm was also investigated using *in-situ* transmission FTIR spectroscopy, which is a vibrational spectroscopy technique that is complementary to SERS. **Figure 2(c)** shows the *in-situ* FTIR spectra collected during exposure of PMVAm to humidified CO<sub>2</sub>/N<sub>2</sub> mixtures as a function of CO<sub>2</sub> partial pressure from 2-98 kPa CO<sub>2</sub>. The full spectrum range from 600 to 4000 cm<sup>-1</sup> is shown in **Figure S7**. The background spectrum for the transmission FTIR spectra was collected under humidified N<sub>2</sub>, which effectively subtracts the bands associated with water vapor and the PMVAm/PP composite membrane; therefore, all bands that appear in **Figure 2(c)** are associated with interactions between PMVAm and CO<sub>2</sub>. There are several FTIR bands observed under all feed CO<sub>2</sub> partial pressures, and the intensity of these bands generally increases with increasing CO<sub>2</sub> partial pressure. As with the SERS spectra, assignment of the FTIR bands is based on literature assignments that are most consistent with our observed band positions. A summary of

the band assignments for the PMVAm samples during exposure to humidified CO<sub>2</sub> gas mixtures is given in **Table 1** with references to the literature.

The FTIR bands located at 1650 cm<sup>-1</sup> (COO<sup>-</sup> asymmetric stretch [19] or C=O stretching from carbamic acid (dimer) [19]) and 1345 cm<sup>-1</sup> (COO<sup>-</sup> asymmetric stretch [14, 19, 21]) are most consistent with bicarbonate species or carbamic acid. The bands located at 1579 cm<sup>-1</sup>, 1446 cm<sup>-1</sup>, and 1395 cm<sup>-1</sup> are consistent with the carbamate ion vibrations of -COO<sup>-</sup> asymmetric [12, 15, 16, 19, 21] and symmetric stretching [12, 13, 15, 16, 19, 21], respectively. The bands located at 1617 cm<sup>-1</sup> and 1479 cm<sup>-1</sup> are consistent with ammonium ions, i.e. NH<sub>2</sub><sup>+</sup> asymmetric [11, 12, 19-22] and symmetric [9, 12, 13, 17, 19, 21] stretching as the carbamate counterion with NH<sup>+</sup> bending [19] also represented by the band at 1479 cm<sup>-1</sup> associated with the bicarbonate ion. Thus, both the Raman and FTIR spectra for PMVAm show bands that are consistent with the formation of both bicarbonate and carbamate species with ammonium species as the counterion.

## 3.2 The Mechanism of CO<sub>2</sub> Transport Across PDVAm (Tertiary Amine)

The structure of PVAm was modified by adding two methyl groups to the primary amine group of PVAm to give PDVAm with tertiary amine groups, as described in Section 2.3, to investigate the influence of amine structure on the CO<sub>2</sub> transport mechanism. The mechanism of CO<sub>2</sub> facilitated transport was then investigated using *operando* SERS and *in-situ* transmission FTIR spectroscopy.

Figure 3(a) shows the effect of feed CO<sub>2</sub> partial pressure on the CO<sub>2</sub> permeance and CO<sub>2</sub>/CH<sub>4</sub> selectivity of PDVAm during exposure to humidified CO<sub>2</sub>/CH<sub>4</sub> mixtures with 2-99 kPa CO<sub>2</sub>, 2.2 kPa H<sub>2</sub>O, and balance CH<sub>4</sub>. Similar to the behavior observed for PMVAm (Figure 2(a)) and PVAm [32], the CO<sub>2</sub> permeance and CO<sub>2</sub>/CH<sub>4</sub> selectivity both decrease with increasing CO<sub>2</sub> partial pressure, suggesting that the tertiary amine groups of PDVAm facilitate transport of CO<sub>2</sub>.

The CO<sub>2</sub> permeance exhibited a maximum value of 418 GPU, while the CO<sub>2</sub>/CH<sub>4</sub> selectivity reached its peak of 129 when the CO<sub>2</sub> partial pressure was maintained at 2 kPa.

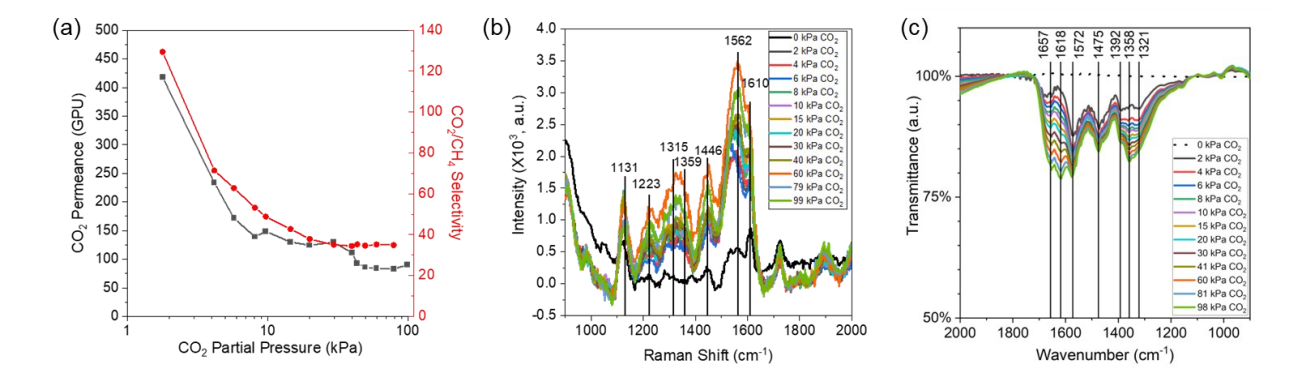


**Figure 3**. CO<sub>2</sub> separation performance and *operando* spectroscopic measurements as a function of feed CO<sub>2</sub> partial pressure for PDVAm where (a) shows the CO<sub>2</sub> permeance (black; left axis) and CO<sub>2</sub>/CH<sub>4</sub> selectivity (red; right axis) and (b) shows the *operando* SERS spectra collected during exposure to a humidified CO<sub>2</sub>/CH<sub>4</sub> feed with 2-99 kPa CO<sub>2</sub>, 2.2 kPa H<sub>2</sub>O, and balance CH<sub>4</sub> at atmospheric pressure and room temperature. (c) *In-situ* transmission FTIR spectra collected during exposure of PDVAm to humidified CO<sub>2</sub>/N<sub>2</sub> with 2-98 kPa CO<sub>2</sub>, 3.7 kPa H<sub>2</sub>O, and balance N<sub>2</sub>.

Figure 3(b) shows the *operando* SERS spectra collected while the CO<sub>2</sub> permeances and CO<sub>2</sub>/CH<sub>4</sub> selectivities in Figure 3(a) were measured during exposure of PDVAm to humidified CO<sub>2</sub>/CH<sub>4</sub> mixtures. The SERS spectra show several overlapping Raman bands that appear in the 1100 cm<sup>-1</sup> to 1700 cm<sup>-1</sup> range, which were not present prior to introducing CO<sub>2</sub> (0 kPa CO<sub>2</sub> spectrum), and their intensity roughly increases with increasing CO<sub>2</sub> partial pressure. To deconvolute the Raman bands, the spectrum collected during exposure to humidified 99 kPa CO<sub>2</sub> was normalized by subtracting the spectrum collected with 0 kPa CO<sub>2</sub>, and the spectrum was fit to seven Gaussian-shaped peaks (Figure S8). Assignment of these peaks is based on comparison of peak positions to the literature. The Raman peaks and their assignment with references to the literature are summarized in Table 2.

**Table 2.** Raman and IR bands formed during exposure to humidified CO<sub>2</sub> and their assignments for PDVAm.

Raman Shifts (cm <sup>-1</sup> )	Wavenumber (cm <sup>-1</sup> )	Band Assignment	Attributed	Refs.
	1657	COO asymmetric stretching from bicarbonate	Bicarbonate Ion	[19]
	1618	NH <sub>2</sub> <sup>+</sup> or NH <sub>3</sub> <sup>+</sup> asymmetric bending, or NH deformation	Ammonium Ion	[11, 12, 19- 22]
1610		C-O antisymmetric stretch of bicarbonate	Bicarbonate Ion	[18, 40, 41, 43-45]
1562		Antisymmetric COO- stretch of carbamate ion	Carbamate Ion	[14, 39, 43]
	1572	-COO <sup>-</sup> asymmetric stretching from carbamate	Carbamate Ion	[10, 12, 13, 19]
1446	1475	NH <sup>+</sup> bending	Ammonium Ion	[19]
	1392	-COO <sup>-</sup> symmetric stretching	Carbamate Ion	[12, 15, 16, 19, 21]
1359	1358	COO <sup>-</sup> symmetric stretching from bicarbonate	Bicarbonate Ion	[18, 38-45] [14, 19, 21]
1315		C-OH bend from bicarbonate	Bicarbonate Ion	[14, 18, 38- 40, 42-44]
	1321	NCOO <sup>-</sup> skeletal vibrations from carbamate	Carbamate Ion	[10, 11, 14, 17, 21-23, 48]
1223		Unknown	Unknown	- 1
1131		C-N-C asymmetric stretching of ammonium ion or neutral secondary amine or CN stretching of carbamate	Ammonium Ion or neutral secondary amine or carbamate	[40, 46] [40, 42, 43, 49- 53]

The Raman bands observed at 1315 cm<sup>-1</sup>, 1359 cm<sup>-1</sup>, and 1610 cm<sup>-1</sup> can be assigned to bicarbonate species [14, 18, 39, 40]. A band at 1562 cm<sup>-1</sup> was also observed, which can be assigned as the carbamate species formed by primary and secondary amines [14, 39, 43]. According to the literature [39, 54], tertiary amines should not react directly with CO<sub>2</sub> to form a NCOO- derivative

due to the instability of the carbamate species related to the high degree of steric hindrance at the nitrogen atom of a tertiary amine. Tertiary amines are expected to react with CO<sub>2</sub> and H<sub>2</sub>O to form bicarbonates through an acid-base reaction, equation (4) [33]. The observation of carbamate species in the *operando* SERS spectra of PDVAm may indicate an incomplete or partial conversion of PVAm to PDVAm. While characterization of PDVAm using FTIR and <sup>1</sup>H NMR (see Section 2.2) is consistent with the PDVAm structure, it is possible that the synthesized polymer may contain a small but significant amount of primary and/or secondary amine groups that can react with CO<sub>2</sub> to form carbamate species. Thus, the band at 1131 cm<sup>-1</sup> could be contributed by the C-N-C asymmetric stretching of ammonium ion [40, 46] or neutral secondary amine [40, 46] or CN stretching of carbamate [40, 42, 43, 49-53], or some combination thereof. The band at 1446 cm<sup>-1</sup> may be assigned to the NH<sup>+</sup> bending of ammonium ion [19]. The band at 1223 cm<sup>-1</sup> is difficult to assign but may be associated with an intermediate that has not been reported in the literature.

To complement *operando* SERS measurements, a PDVAm membrane was also analyzed by *in-situ* transmission FTIR spectroscopy during exposure to humidified CO<sub>2</sub>/N<sub>2</sub> mixtures with 2-98 kPa CO<sub>2</sub>, 3.7 kPa H<sub>2</sub>O, and balance N<sub>2</sub>. **Figure 3(c)** shows the transmission FTIR spectra in the 900-2000 cm<sup>-1</sup> range with the full spectral range (600-4000 cm<sup>-1</sup>) shown in **Figure S9**. The *in-situ* transmission FTIR spectra display several bands in the fingerprint region; the background spectrum for the transmission FTIR spectra was collected under humidified N<sub>2</sub>, and therefore all bands in **Figure 3(c)** are associated with species resulting from the interactions of CO<sub>2</sub> with PDVAm. The positions and assignments of the bands with references to the literature are summarized in **Table 2**.

The FTIR spectra of PDVAm reveal bands located at 1657 cm<sup>-1</sup> (COO<sup>-</sup> asymmetric stretching [19]) and 1358 cm<sup>-1</sup> (COO<sup>-</sup> symmetric stretching [14, 19, 21]) which are consistent with

bicarbonate ions with the band located at 1475 cm<sup>-1</sup> (NH<sup>+</sup> bending [19]) representing the ammonium counterion to bicarbonate. There are also bands located at 1572 cm<sup>-1</sup> (-COO<sup>-</sup> asymmetric stretching [10, 12, 13, 19]), 1392 cm<sup>-1</sup> (-COO<sup>-</sup> symmetric stretching [12, 15, 16, 19, 21]), and 1321 cm<sup>-1</sup> (NCOO<sup>-</sup> skeletal vibrations [11, 12, 19-22]) that are consistent with the carbamate species; the band at 1618 cm<sup>-1</sup> (NH<sub>2</sub><sup>+</sup> or NH<sub>3</sub><sup>+</sup> asymmetric bending [11, 12, 19-22]) is consistent with the ammonium counterion to the carbamate species. However, NH<sub>2</sub><sup>+</sup> or NH<sub>3</sub><sup>+</sup> will not form with a tertiary amine and there are no other relevant assignments for a tertiary amine, to our knowledge. The most likely explanation is that PVAm was not fully converted into PDVAm, and the synthesized polymer contained a significant amount of primary and/or secondary amine groups, as discussed above. In general, the FTIR results are consistent with the SERS results and both demonstrate that CO<sub>2</sub> moves across PDVAm as both carbamate and bicarbonate species.

## 3.3 The Mechanism of CO<sub>2</sub> Transport Across P4VP (Pyridinic Amine)

In addition to the PVAm-derived secondary (PMVAm) and tertiary (PDVAm) amine-functionalized polymers, the mechanism of CO<sub>2</sub> transport across P4VP, which has pyridinic amine groups (see **Figure 1**), was also investigated using *operando* SERS and *in-situ* FTIR spectroscopy to gain broader insight into the influence of the structure of the amine group on the CO<sub>2</sub> transport mechanism. **Figure 4(a)** shows the CO<sub>2</sub> permeance and CO<sub>2</sub>/CH<sub>4</sub> selectivity of P4VP versus CO<sub>2</sub> partial pressure during exposure to 2-99 kPa CO<sub>2</sub>, 2.2 kPa H<sub>2</sub>O, and balance CH<sub>4</sub> at atmospheric pressure. Similar to the behavior observed for PVAm [32], PMVAm (Figure 2(a)) and PDVAm (Figure 3(a)), the CO<sub>2</sub> permeance and the CO<sub>2</sub>/CH<sub>4</sub> selectivity of P4VP decreases with increasing CO<sub>2</sub> partial pressure, indicating facilitated transport of CO<sub>2</sub>.

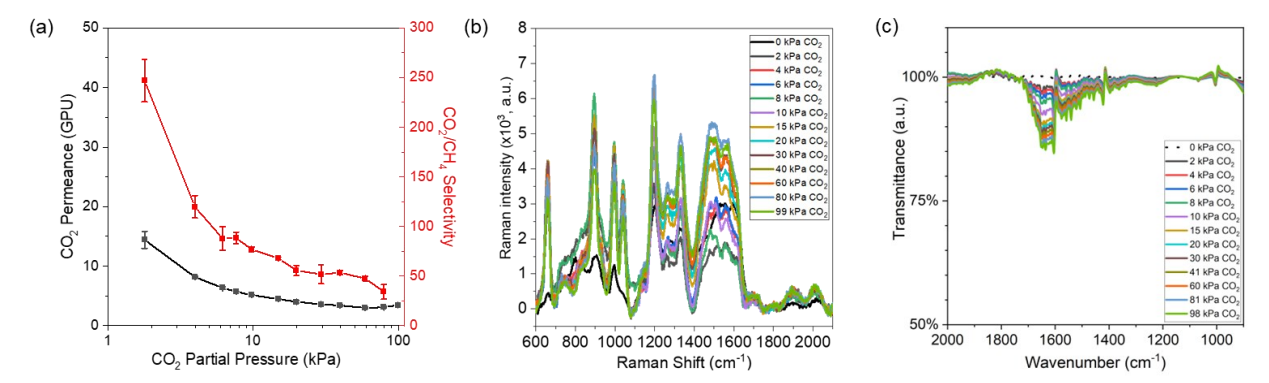


**Figure 4.** CO<sub>2</sub> separation performance and *operando* spectroscopic measurements as a function of feed CO<sub>2</sub> partial pressure for P4VP where (a) shows the CO<sub>2</sub> permeance (black; left axis) and CO<sub>2</sub>/CH<sub>4</sub> selectivity (red; right axis) and (b) shows the *operando* SERS spectra during exposure to a humidified CO<sub>2</sub>/CH<sub>4</sub> feed with 2-99 kPa CO<sub>2</sub>, 2.2 kPa H<sub>2</sub>O, and balance CH<sub>4</sub> at atmospheric pressure and room temperature. (c) *In-situ* transmission FTIR spectra collected during exposure to humidified CO<sub>2</sub>/N<sub>2</sub> with 2-98 kPa CO<sub>2</sub>, 3.7 kPa H<sub>2</sub>O, and balance N<sub>2</sub>.

373 374

375376

377378

379

380

381

382

383

384

385

386

387

388

389

390

391

392

393

394

The operando SERS spectra collected during exposure of P4VP to humidified CO<sub>2</sub>/CH<sub>4</sub> mixtures, which are shown in **Figure 4(b)**, display many bands that generally increase in intensity with increasing CO<sub>2</sub> partial pressure. These bands were not observed in the corresponding SERS spectra of PVAm, PMVAm, or PDVAm, and are not consistent with either carbamate or bicarbonate species. A rough assignment of these bands is given in Table S2. The bands at 658 cm<sup>-1</sup>, 1042 cm<sup>-1</sup>, 1195 cm<sup>-1</sup>, and 1479 cm<sup>-1</sup> are similar to the positions of bands assigned in the literature to P4VP (650 cm<sup>-1</sup>, 1012 cm<sup>-1</sup>, 1209 cm<sup>-1</sup>, and 1445 cm<sup>-1</sup>) [55]. The bands at 996 cm<sup>-1</sup>, 1195 cm<sup>-1</sup> and 1594 cm<sup>-1</sup> are similar to the positions of SERS bands assigned in the literature to P4VP adsorbed onto silver island films (1020 cm<sup>-1</sup>, 1219 cm<sup>-1</sup>, and 1613 cm<sup>-1</sup>), which may indicate that the pyridine moieties of P4VP are adsorbed onto the surface of silver nanoparticles embedded in the P4VP film [56]. There are also several bands (658 cm<sup>-1</sup>, 1195 cm<sup>-1</sup>, 1264 cm<sup>-1</sup>, 1334 cm<sup>-1</sup>, and 1594 cm<sup>-1</sup>) that are close in position to Raman bands assigned in the literature to protonated 4-ethylpyridine Raman bands (652 cm<sup>-1</sup>, 1204 cm<sup>-1</sup>, 1265 cm<sup>-1</sup>, 1315 cm<sup>-1</sup> and 1607 cm<sup>-1</sup>) [55]. This may suggest that some of the pyridine rings of P4VP are protonated under operating conditions. Since the band at 658 cm<sup>-1</sup> from neutral pyridine in P4VP is very weak, according to

the literature [55], the high intensity of this band in our spectra may indicate a protonated pyridine ring. Overall, the *operando* SERS spectra are dominated by features that can be assigned to the pyridine ring of P4VP and no carbamate or bicarbonate species were detected.

The *in-situ* transmission FTIR spectra of P4VP collected during exposure to humidified CO<sub>2</sub>/N<sub>2</sub> with 2-98 kPa CO<sub>2</sub>, 3.7 kPa H<sub>2</sub>O, and balance N<sub>2</sub>, which are shown in Figure 4(c) with the full spectral range shown in Figure S10, are also much different than the corresponding FTIR spectra of PVAm [32], PMVAm, and PDVAm. Furthermore, while there were many bands observed in the operando SERS spectra of P4VP (Figure 4(a)), there was only one broad, poorlydefined band in the *in-situ* transmission FTIR spectra of P4VP. This band centered at ~1640 cm<sup>-1</sup> is most likely associated with a bending mode of water [57, 58]. There is also some evidence of derivative-shaped bands that could result from a shift in the bands associated with the pyridine ring of P4VP from weak interactions with water or CO<sub>2</sub> [59-62]. Thus, while the operando SERS spectra and *in-situ* transmission FTIR spectra display many different features, analysis of both sets of spectra both suggests that CO<sub>2</sub> is not converted to carbamate or bicarbonate. Rather, our results suggest that CO<sub>2</sub> interacts weakly with the pyridinic nitrogen atoms of P4VP. Permeation results (Figure 4(a)) suggest that the pyridinic nitrogen atoms of P4VP facilitate CO<sub>2</sub> transport; operando SERS and in-situ FTIR results suggest that facilitated transport can occur even through weak interactions of amine groups with CO<sub>2</sub> and without conversion of CO<sub>2</sub> to carbamate or bicarbonate intermediates.

#### 4. Conclusions

395

396

397

398

399

400

401

402

403

404

405

406

407

408

409

410

411

412

413

414

415

416

This work demonstrates that the interaction of CO<sub>2</sub> with amine-functionalized membranes, and hence the mechanism of CO<sub>2</sub> facilitated transport, is highly sensitive to the molecular structure

of the amine site. While this is not a surprising result, it is important to directly observe these interactions to understand the molecular-level details of CO<sub>2</sub> facilitated transport for rational design of high-performance membranes. To more clearly show the differences in the interaction of CO<sub>2</sub> with the different polymers, **Figure 5** shows a comparison of the (a) *operando* SERS and (b) *in-situ* transmission FTIR spectra collected during exposure of PVAm, PMVAm, PDVAm, and P4VP to 20 kPa CO<sub>2</sub>, 3.7 kPa H<sub>2</sub>O, and balance N<sub>2</sub>.

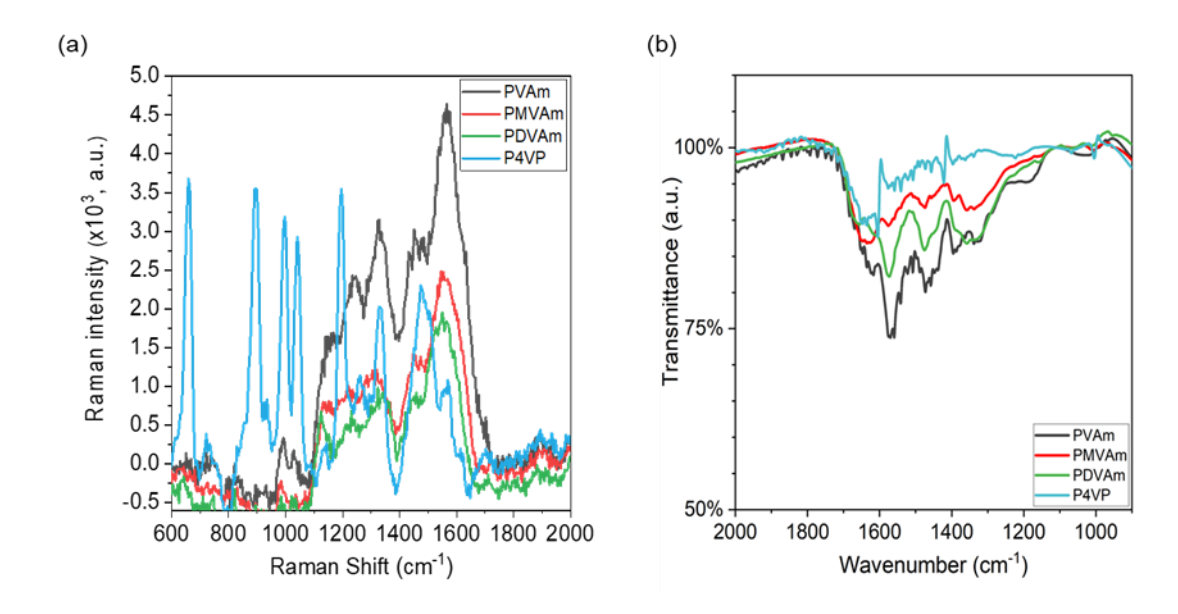


**Figure 5**. (a) *Operando* Raman spectra and (b) *In-situ* transmission FTIR spectra of PVAm (black), PMVAm (red), PDVAm (green), and P4VP (blue) polymers collected during exposure to humidified CO<sub>2</sub>/N<sub>2</sub> mixtures at 20 kPa CO<sub>2</sub>, 3.7 kPa H<sub>2</sub>O, and balance N<sub>2</sub>. The FTIR spectrum of PVAm was reported in a previous publication [30].

W hile CO<sub>2</sub> moves across PVAm primarily by hopping from one primary amine site to another as carbamate species, our results suggest that CO<sub>2</sub> moves across PMVAm and PDVAm with secondary and tertiary amine sites, respectively, as a mixture of both carbamate and

bicarbonate species. The observation of carbamate intermediates formed in PDVAm with tertiary amines was surprising, as carbamate species are not expected to be stable on tertiary amines, as discussed in Section 3.2. However, this may be explained by an incomplete conversion of PVAm to PDVAm, and there may be some primary and/or secondary amine sites that may interact with CO<sub>2</sub> to form carbamates. Perhaps the most significant finding from this work was the observation that P4VP may be capable of facilitating CO<sub>2</sub> transport by weak interactions with CO<sub>2</sub> rather than by converting CO<sub>2</sub> to carbamate or bicarbonate species. This is a new facilitated CO<sub>2</sub> transport mechanism that has not been reported in the literature, to our knowledge. It is possible that, in addition to CO<sub>2</sub> facilitated transport via carbamate/bicarbonate intermediates, CO<sub>2</sub> transport across PVAM, PMVAm, and PDVAm is also facilitated by such weak amine-CO<sub>2</sub> interactions.

#### 5. Conflicts of Interest

433

434

435

436

437

438

439

440

441

442

443

445

450

The authors declare no conflicts of interest.

#### 6. Acknowledgments

- 446 Acknowledgments are made to the Donors of the American Chemical Society Petroleum Research
- Fund, the NSF CAREER (Grant Number CBET-2144362), the Department of Education (Grant
- Number P200A210048), College of Engineering at the University of Notre Dame, and the
- Graduate School at the University of Notre Dame for support (or partial support) of this research.

#### 7. References

- 451 [1] Y. Zhao, W.S. Winston Ho, Steric Hindrance Effect on Amine Demonstrated In Solid Polymer
- 452 Membranes for CO<sub>2</sub> Transport, J. Membr. Sci. 415-416 (2012) 132-138.
- 453 https://doi.org/https://doi.org/10.1016/j.memsci.2012.04.044.
- 454 [2] Y. Zhao, W.S.W. Ho, CO2-Selective Membranes Containing Sterically Hindered Amines for
- 455 CO<sub>2</sub>/H<sub>2</sub> Separation, Ind. Eng. Chem. Res. 52(26) (2013) 8774-8782.
- 456 <a href="https://doi.org/10.1021/ie301397m">https://doi.org/10.1021/ie301397m</a>.

- 457 [3] Z. Tong, W.S.W. Ho, New Sterically Hindered Polyvinylamine Membranes for CO<sub>2</sub> Separation
- 458 and Capture, J. Membr. Sci. 543 (2017) 202-211.
- 459 https://doi.org/https://doi.org/10.1016/j.memsci.2017.08.057.
- 460 [4] M. Caplow, Kinetics of Carbamate Formation and Breakdown, J. Am. Chem. Soc. 90(24) (1968)
- 461 6795-6803. https://doi.org/10.1021/ja01026a041.
- 462 [5] P.V. Danckwerts, The Reaction of CO<sub>2</sub> with Ethanolamines, Chem. Eng. Sci. 34(4) (1979) 443-
- 463 446. https://doi.org/https://doi.org/10.1016/0009-2509(79)85087-3.
- 464 [6] A.K. Chakraborty, G. Astarita, K.B. Bischoff, CO<sub>2</sub> Absorption in Aqueous Solutions of Hindered
- 465 Amines, Chem. Eng. Sci. 41(4) (1986) 997-1003. <a href="https://doi.org/https://doi.org/10.1016/0009-466">https://doi.org/https://doi.org/10.1016/0009-466</a> 2509(86)87185-8.
- 467 [7] P. Tontiwachwuthikul, A. Meisen, C.J. Lim, CO<sub>2</sub> Absorption by NaOH, Monoethanolamine and
- 468 2-amino-2-methyl-1-propanol Solutions in A Packed Column, Chem. Eng. Sci. 47(2) (1992) 381-
- 469 390. <a href="https://doi.org/https://doi.org/10.1016/0009-2509(92)80028-B">https://doi.org/https://doi.org/10.1016/0009-2509(92)80028-B</a>.
- 470 [8] J.-Y. Park, S.J. Yoon, H. Lee, Effect of Steric Hindrance on Carbon Dioxide Absorption into
- 471 New Amine Solutions: Thermodynamic and Spectroscopic Verification through Solubility and
- 472 NMR Analysis, Environ. Sci. Technol. 37(8) (2003) 1670-1675.
- 473 https://doi.org/10.1021/es0260519.
- 474 [9] M.W. Hahn, M. Steib, A. Jentys, J.A. Lercher, Mechanism and Kinetics of CO<sub>2</sub> Adsorption on
- 475 Surface Bonded Amines, J. Phys. Chem. C 119(8) (2015) 4126-4135
- 476 <a href="https://doi.org/10.1021/jp512001t">https://doi.org/10.1021/jp512001t</a>.
- 477 [10] J. Yu, S.S.C. Chuang, The Structure of Adsorbed Species on Immobilized Amines in CO<sub>2</sub>
- 478 Capture: An in Situ IR Study, Energy Fuels 30(9) (2016) 7579-7587.
- https://doi.org/10.1021/acs.energyfuels.6b01423.
- 480 [11] S. Chakravartula Srivatsa, S. Bhattacharya, Amine-Based CO<sub>2</sub> Capture Sorbents: A Potential
- 481 CO<sub>2</sub> Hydrogenation Catalyst, J. CO<sub>2</sub> Util. 26 (2018) 397-407.
- 482 <a href="https://doi.org/https://doi.org/10.1016/j.jcou.2018.05.028">https://doi.org/https://doi.org/https://doi.org/10.1016/j.jcou.2018.05.028</a>.
- 483 [12] A. Danon, P.C. Stair, E. Weitz, FTIR Study of CO<sub>2</sub> Adsorption on Amine-Grafted SBA-15:
- 484 Elucidation of Adsorbed Species, J. Phys. Chem. C 115(23) (2011) 11540-11549.
- 485 https://doi.org/10.1021/jp200914v.
- 486 [13] Z. Bacsik, N. Ahlsten, A. Ziadi, G. Zhao, A.E. Garcia-Bennett, B. Martín-Matute, N. Hedin,
- Mechanisms and Kinetics for Sorption of CO<sub>2</sub> on Bicontinuous Mesoporous Silica Modified with
- 488 n-Propylamine, Langmuir 27(17) (2011) 11118-11128. <a href="https://doi.org/10.1021/la202033p">https://doi.org/10.1021/la202033p</a>.
- 489 [14] G. Richner, G. Puxty, Assessing the Chemical Speciation during CO2 Absorption by Aqueous
- 490 Amines Using in Situ FTIR, Ind. Eng. Chem. Res. 51(44) (2012) 14317-14324.
- 491 https://doi.org/10.1021/ie302056f.
- 492 [15] J.-B. Bossa, P. Theulé, F. Duvernay, F. Borget, T. Chiavassa, Carbamic Acid and Carbamate
- Formation in NH: CO ices–UV Irradiation Versus Thermal Processes, Astron. Astrophys. 492(3) 494 (2008) 719-724.
- 494 (2006) / 19-724
- 495 [16] C. Knöfel, C. Martin, V. Hornebecq, P.L. Llewellyn, Study of Carbon Dioxide Adsorption on
- 496 Mesoporous Aminopropylsilane-Functionalized Silica and Titania Combining Microcalorimetry
- 497 and in Situ Infrared Spectroscopy, J. Phys. Chem. C 113(52) (2009) 21726-21734.
- 498 https://doi.org/10.1021/jp907054h.
- 499 [17] M.W. Hahn, J. Jelic, E. Berger, K. Reuter, A. Jentys, J.A. Lercher, Role of Amine Functionality
- for CO<sub>2</sub> Chemisorption on Silica, The Journal of Physical Chemistry B 120(8) (2016) 1988-1995.
- 501 <a href="https://doi.org/10.1021/acs.jpcb.5b10012">https://doi.org/10.1021/acs.jpcb.5b10012</a>.
- [18] J.J. Lee, C.-H. Chen, D. Shimon, S.E. Hayes, C. Sievers, C.W. Jones, Effect of Humidity on
- the CO<sub>2</sub> Adsorption of Tertiary Amine Grafted SBA-15, J. Phys. Chem. C 121(42) (2017) 23480-
- 504 23487. https://doi.org/10.1021/acs.jpcc.7b07930.
- 505 [19] G.S. Foo, J.J. Lee, C.-H. Chen, S.E. Hayes, C. Sievers, C.W. Jones, Elucidation of Surface
- 506 Species through in Situ FTIR Spectroscopy of Carbon Dioxide Adsorption on Amine-Grafted SBA-
- 507 15, ChemSusChem 10(1) (2017) 266-276. https://doi.org/https://doi.org/10.1002/cssc.201600809.

- 508 [20] Y. Zhai, S.S.C. Chuang, The Nature of Adsorbed Carbon Dioxide on Immobilized Amines
- during Carbon Dioxide Capture from Air and Simulated Flue Gas, Energy Technol. 5(3) (2017)
- 510 510-519. https://doi.org/https://doi.org/10.1002/ente.201600685.
- 511 [21] S.A. Didas, M.A. Sakwa-Novak, G.S. Foo, C. Sievers, C.W. Jones, Effect of Amine Surface
- 512 Coverage on the Co-Adsorption of CO<sub>2</sub> and Water: Spectral Deconvolution of Adsorbed Species,
- 513 J. Phys. Chem. Lett. 5(23) (2014) 4194-4200. https://doi.org/10.1021/jz502032c.
- 514 [22] U. Tumuluri, M. Isenberg, C.-S. Tan, S.S.C. Chuang, In Situ Infrared Study of the Effect of
- Amine Density on the Nature of Adsorbed CO<sub>2</sub> on Amine-Functionalized Solid Sorbents, Langmuir
- 516 30(25) (2014) 7405-7413. https://doi.org/10.1021/la501284y.
- 517 [23] W.C. Wilfong, C.S. Srikanth, S.S.C. Chuang, In Situ ATR and DRIFTS Studies of the Nature
- of Adsorbed CO<sub>2</sub> on Tetraethylenepentamine Films, ACS Appl. Mater. Interfaces 6(16) (2014)
- 519 13617-13626. https://doi.org/10.1021/am5031006.
- 520 [24] C.P. O'Brien, A Perspective on the Application of Operando Characterization to Probe The
- 521 Structure, Performance, and Dynamics of Membranes under Realistic Operating Conditions, J.
- 522 Membr. Sci. 619 (2021) 118751. <a href="https://doi.org/https://doi.org/10.1016/j.memsci.2020.118751">https://doi.org/https://doi.org/10.1016/j.memsci.2020.118751</a>.
- [25] C.P. O'Brien, Z.W. Dunbar, I.C. Lee, A Spectroscopic Membrane Permeation Cell for In-situ
- 524 Infrared-reflection Absorption Spectroscopic Analysis of Membrane Surfaces and Simultaneous
- Measurement of Trans-membrane Gas Permeation Rates, J. Membr. Sci. 526 (2017) 43-51.
- 526 https://doi.org/https://doi.org/10.1016/j.memsci.2016.12.016.
- 527 [26] C.P. O'Brien, I.C. Lee, The Interaction of CO with PdCu Hydrogen Separation Membranes:
- 528 An Operando Infrared Spectroscopy Study, Catal. Today 336 (2019) 216-222.
- 529 <u>https://doi.org/https://doi.org/10.1016/j.cattod.2017.09.039</u>.
- [27] C.P. O'Brien, I.C. Lee, CO Poisoning and CO Hydrogenation on the Surface of Pd Hydrogen
- 531 Separation Membranes, J. Phys. Chem. C 121(31) (2017) 16864-16871.
- 532 <a href="https://doi.org/10.1021/acs.jpcc.7b05046">https://doi.org/10.1021/acs.jpcc.7b05046</a>.
- [28] G. Lee, J. Easa, R. Jin, A. Booth, C.P. O'Brien, Enhancing the Surface Sensitivity of In-
- 534 situ/Operando Characterization of Palladium Membranes through Polarization Modulation and
- Synthesis of Optically Smooth Palladium Thin Films, J. Membr. Sci. 637 (2021) 119605.
- 536 <a href="https://doi.org/https://doi.org/10.1016/j.memsci.2021.119605">https://doi.org/https://doi.org/10.1016/j.memsci.2021.119605</a>.
- 537 [29] C.P. O'Brien, I.C. Lee, Z.W. Dunbar, Spectroscopic Membrane Permeation Cell for
- Simultaneous Measurements of Gas Permeation Rates and Infrared Reflection Absorption
- 539 Spectroscopic Analysis of Membrane Surfaces, U.S. Patent No. 10,663,389, 2020.
- 540 [30] S.G. Pate, H. Xu, C.P. O'Brien, Operando Observation of CO<sub>2</sub> Transport Intermediates in
- 541 Polyvinylamine Facilitated Transport Membranes, and the Role of Water in the Formation of
- Intermediates, Using Transmission FTIR Spectroscopy, J. Mater. Chem. A 10(8) (2022) 4418-
- 543 4427. <a href="https://doi.org/10.1039/D1TA10015G">https://doi.org/10.1039/D1TA10015G</a>.
- 544 [31] H. Xu, J. Easa, S.G. Pate, R. Jin, C.P. O'Brien, Operando Surface-Enhanced Raman-
- Scattering (SERS) for Probing CO<sub>2</sub> Facilitated Transport Mechanisms of Amine-Functionalized
- 546 Polymeric Membranes, ACS Appl. Mater. Interfaces 14(13) (2022) 15697-15705.
- 547 https://doi.org/10.1021/acsami.2c02769.
- 548 [32] H. Xu, S.G. Pate, C.P. O'Brien, Mathematical Modeling of CO<sub>2</sub> Facilitated Transport across
- 549 Polyvinylamine Membranes with Direct Operando Observation of Amine Carrier Saturation, Chem.
- 550 Eng. J. 460 (2023) 141728. https://doi.org/https://doi.org/10.1016/j.cej.2023.141728.
- [33] Y. Han, W.W. Ho, Recent advances in polymeric membranes for CO2 capture, Chin. J. Chem.
- 552 Eng. 26(11) (2018) 2238-2254.
- 553 [34] K.K. Chen, Y. Han, Z. Zhang, W.S.W. Ho, Enhancing Membrane Performance for CO<sub>2</sub>
- Capture from Flue Gas with Ultrahigh MW Polyvinylamine, J. Membr. Sci. 628 (2021) 119215.
- 555 https://doi.org/https://doi.org/10.1016/j.memsci.2021.119215.
- 556 [35] B. Belaissaoui, E. Lasseuguette, S. Janakiram, L. Deng, M.C. Ferrari, Analysis of CO<sub>2</sub>
- 557 Facilitation Transport Effect through a Hybrid Poly(Allyl Amine) Membrane: Pathways for Further
- 558 Improvement, Membranes (Basel) 10(12) (2020). https://doi.org/10.3390/membranes10120367.

- [36] A. Klemm, Y.-Y. Lee, H. Mao, B. Gurkan, Facilitated Transport Membranes With Ionic Liquids for CO<sub>2</sub> Separations, Front. Chem. 8 (2020). https://doi.org/10.3389/fchem.2020.00637.
- 561 [37] H. Guo, J. Wei, Y. Ma, J. Deng, S. Yi, B. Wang, L. Deng, X. Jiang, Z. Dai, Facilitated Transport
- Membranes for CO<sub>2</sub>/CH<sub>4</sub> Separation State of the Art, Adv.Membr. 2 (2022) 100040.
- 563 https://doi.org/https://doi.org/10.1016/j.advmem.2022.100040.
- 564 [38] K. Robinson, A. McCluskey, M.I. Attalla, An ATR-FTIR Study on the Effect of Molecular
- 565 Structural Variations on the CO<sub>2</sub> Absorption Characteristics of Heterocyclic Amines, Part II,
- 566 ChemPhysChem 13(9) (2012) 2331-2341.
- 567 https://doi.org/https://doi.org/10.1002/cphc.201200066.
- 568 [39] K. Robinson, A. McCluskey, M.I. Attalla, An FTIR Spectroscopic Study on the Effect of
- Molecular Structural Variations on the CO<sub>2</sub> Absorption Characteristics of Heterocyclic Amines,
- 570 ChemPhysChem 12(6) (2011) 1088-1099.
- 571 https://doi.org/https://doi.org/10.1002/cphc.201001056.
- 572 [40] N. Wen, M.H. Brooker, Ammonium Carbonate, Ammonium Bicarbonate, and Ammonium
- 573 Carbamate Equilibria: A Raman Study, J. Phys. Chem. 99(1) (1995) 359-368.
- 574 [41] F. Milella, M. Mazzotti, Estimating Speciation of Aqueous Ammonia Solutions of Ammonium
- 575 Bicarbonate: Application of Least Squares Methods to Infrared Spectra, Reaction Chemistry &
- 576 Engineering 4(7) (2019) 1284-1302. <a href="https://doi.org/10.1039/C9RE00137A">https://doi.org/10.1039/C9RE00137A</a>.
- 577 [42] J. Yu, S.S. Chuang, The Structure of Adsorbed Species on Immobilized Amines in CO<sub>2</sub>
- 578 Capture: an in Situ IR Study, Energy Fuels 30(9) (2016) 7579-7587.
- 579 [43] S. Stegmeier, M. Fleischer, A. Tawil, P. Hauptmann, K. Egly, K. Rose, Mechanism of the
- Interaction of CO<sub>2</sub> and Humidity with Primary Amino Group Systems for Room Temperature CO<sub>2</sub>
- 581 Sensors, Procedia Chem. 1(1) (2009) 236-239.
- 582 [44] J.J. Walsh, Investigating the Effects of Pyridine and Poly(4-Vinylpyridine) on CO<sub>2</sub> Reduction
- 583 Electrocatalysis at Gold Electrodes Using in Situ Surface-Enhanced Raman
- 584 Spectroelectrochemistry, Phys. Chem. Chem. Phys. 22(22) (2020) 12766-12771.
- 585 https://doi.org/10.1039/D0CP00632G.
- 586 [45] M.K. Wong, M.A. Bustam, A.M. Shariff, Chemical Speciation of CO<sub>2</sub> Absorption in Aqueous
- Monoethanolamine Investigated by In Situ Raman Spectroscopy, Int. J. Greenh. Gas Control. 39
- 588 (2015) 139-147. https://doi.org/https://doi.org/10.1016/j.ijggc.2015.05.016.
- 589 [46] B.C. Smith, Spectroscopy, Organic Nitrogen Compounds III: Seconday and Tertiary amines
- 590 2019, pp. 22-26.
- 591 [47] J. Yu, Y. Zhai, S.S.C. Chuang, Water Enhancement in CO<sub>2</sub> Capture by Amines: An Insight
- into CO<sub>2</sub>–H<sub>2</sub>O Interactions on Amine Films and Sorbents, Ind. Eng. Chem. Res. 57(11) (2018)
- 593 4052-4062. <a href="https://doi.org/10.1021/acs.iecr.7b05114">https://doi.org/10.1021/acs.iecr.7b05114</a>.
- [48] J. Yu, S.S.C. Chuang, The Role of Water in CO<sub>2</sub> Capture by Amine, Ind. Eng. Chem. Res.
- 595 56(21) (2017) 6337-6347. https://doi.org/10.1021/acs.iecr.7b00715.
- [49] C. Hisatsune, Low-Temperature Infrared Study of Ammonium Carbamate Formation, Can. J.
- 597 Chem. 62(5) (1984) 945-948. https://doi.org/10.1139/V84-155.
- 598 [50] R. Khanna, M. Moore, Carbamic Acid: Molecular Structure and IR Spectra, Spectrochim.
- 599 Acta A Mol. Biomol. Spectrosc. 55(5) (1999) 961-967.
- 600 [51] J.-B. Bossa, F. Borget, F. Duvernay, P. Theulé, T. Chiavassa, Formation of Neutral
- 601 Methylcarbamic Acid (CH<sub>3</sub>NHCOOH) and Methylammonium Methylcarbamate
- 602  $[CH_3NH_3^+][CH_3NHCO_2^-]$  at Low Temperature, J. Phys. Chem. A 112(23) (2008) 5113-5120.
- 603 https://doi.org/10.1021/JP800723C.
- [52] Z. Idris, K.J. Jens, D.A. Eimer, Speciation of Mea-CO<sub>2</sub> Adducts at Equilibrium Using Raman
- 605 Spectroscopy, Energy Procedia 63 (2014) 1424-1431.
- 606 [53] F. Milella, M. Mazzotti, Estimating Speciation of Aqueous Ammonia Solutions of Ammonium
- Bicarbonate: Application of Least Squares Methods to Infrared Spectra, React. Chem. Eng. 4(7)
- 608 (2019) 1284-1302. https://doi.org/10.1039/C9RE00137A.

- [54] Y. Han, W.S.W. Ho, Recent Advances in Polymeric Membranes for CO<sub>2</sub> Capture, Chin. J.
- 610 Chem. Eng. 26(11) (2018) 2238-2254. https://doi.org/https://doi.org/10.1016/j.cjche.2018.07.010.
- 611 [55] R.L. Garrell, K.D. Beer, Surface-enhanced Raman Scattering from 4-ethylpyridine and
- 612 Poly(4-vinylpyridine) on Gold and Silver Electrodes, Langmuir 5(2) (1989) 452-458.
- 613 https://doi.org/10.1021/la00086a029.
- [56] P.G. Roth, F.J. Boerio, Surface-enhanced Raman Scattering from Poly(4-vinyl pyridine), J.
- 615 Polym. Sci. B Polym. Phys. 25(9) (1987) 1923-1933.
- 616 https://doi.org/https://doi.org/10.1002/polb.1987.090250912.
- 617 [57] C.S. Srikanth, S.S.C. Chuang, Spectroscopic Investigation into Oxidative Degradation of
- 618 Silica-Supported Amine Sorbents for CO<sub>2</sub> Capture, ChemSusChem 5(8) (2012) 1435-1442.
- 619 https://doi.org/https://doi.org/10.1002/cssc.201100662.
- [58] E. Garand, T. Wende, D.J. Goebbert, R. Bergmann, G. Meijer, D.M. Neumark, K.R. Asmis,
- Infrared Spectroscopy of Hydrated Bicarbonate Anion Clusters: HCO<sub>3</sub><sup>-</sup>(H<sub>2</sub>O)<sub>1-10</sub>, J. Am. Chem.
- 622 Soc. 132(2) (2010) 849-856. https://doi.org/10.1021/ja9093132.
- 623 [59] R. Jin, H. Xu, J. Easa, A. Chapero-Planell, C.P. O'Brien, Cycloaddition of CO<sub>2</sub> to
- 624 Epichlorohydrin over Pyridine, Vinylpyridine, and Poly(vinylpyridine): The Influence of Steric
- 625 Crowding on the Reaction Mechanism, J. Phys. Chem. C 127(3) (2023) 1441-1454.
- 626 <a href="https://doi.org/10.1021/acs.jpcc.2c08516">https://doi.org/10.1021/acs.jpcc.2c08516</a>.
- 627 [60] S.W. Lee, B. Chae, S.G. Hahm, B. Lee, S.B. Kim, M. Ree, Rubbed Films of isomeric Poly(4-
- of vinylpyridine) and Poly(2-vinylpyridine): Surface Morphology, Molecular Orientation, and Liquid
- 629 Crystal Alignability, Polymer 46(12) (2005) 4068-4076.
- 630 <a href="https://doi.org/https://doi.org/10.1016/j.polymer.2005.03.085">https://doi.org/https://doi.org/10.1016/j.polymer.2005.03.085</a>.
- [61] K. Mavronasou, A. Zamboulis, P. Klonos, A. Kyritsis, D.N. Bikiaris, R. Papadakis, I. Deligkiozi,
- Poly(vinyl pyridine) and Its Quaternized Derivatives: Understanding Their Solvation and Solid
- 633 State Properties, Polymers 14(4) (2022) 804.

637

- 634 [62] J. Li, X. Ou, S. Sims, W. Li, L. Wu, Hybrid Liquid Crystal Polymers from the Self-Assembly of
- Poly(vinylpyridine) and Polyoxometalates via Multiple Non-Covalent Bonds, RSC Adv. 4(100)
- 636 (2014) 56998-57008. https://doi.org/10.1039/C4RA12174K.